



Size-dependent Mohr–Coulomb failure criterion

Yun Zhao¹ · Brijes Mishra² · Qingwen Shi¹ · Gaobo Zhao¹

Received: 16 November 2022 / Accepted: 28 April 2023
© Springer-Verlag GmbH Germany, part of Springer Nature 2023

Abstract

Numerous experimental results show the compressive strength of rock decreases with the increase of rock size. Researchers have developed different empirical failure criteria to correlate the decreasing size effect of compressive strength. For the first time, this research theoretically derived the size-dependent Mohr–Coulomb failure criterion based on the Griffith theory. The failure criterion contains three parameters: the cohesion, the friction angle, and the scaling exponent, which can be determined based on the uniaxial compression test of different-sized specimens and the triaxial compression test of standard-sized specimens. The determined failure criterion can be used to predict the compressive strength of different-sized rocks at different compressive stress conditions. This failure criterion demonstrates that the cracks inside rock cause the size effect, and the crack length distribution affects the size effect. Next, this research developed the bonded-particle model of rock to verify the failure criterion. The rock model consists of matrix and cracks that are modeled by bonded particles and discrete fractures, respectively. The modeling result shows that the strength of matrix model is size independent, and the introduction of cracks causes the size effect of rock model. The parametric analysis verified the influence of crack length distribution on the size effect according to the failure criterion. At last, this research summarized the experimental data of uniaxial and triaxial compressive strength in previous size effect research to check the applicability of the failure criterion. The fitting result shows the failure criterion fits well with the experimental data. Moreover, this research found experimental evidence to support the failure criterion.

Keywords Size effect · Compressive strength · Mohr–Coulomb failure criterion · Griffith theory · Bonded-particle model

Introduction

Obtaining the strength of large-sized rock is a long-standing challenge (Peng 2015). Researchers have rarely measured rock strength directly in the field due to the high cost of in situ testing and the capability of test machines (Shi et al. 2022). A common practice is to estimate the strength of large-sized rock from laboratory testing conducted on small-sized rock according to the size effect of rock strength.

Researchers have conducted extensive studies into the size effect of rock strength.

The uniaxial compressive strength (UCS) is one of the most important mechanical parameters in rock engineering. There are many studies on the size effect of UCS showing that the UCS decreases as size increases (Abou-Sayed and Brechtel 1976; Baecher and Einstein 1981; Bieniawski 1968; Darlington et al. 2011; Gonzatti et al. 2014; Herget and Unrug 1976; Hoskins and Horino 1969; Jackson and Lau 1990; Jahns 1966; Kong et al. 2021; Li 2019; Lundborg 1967; Mogi 1962; Natau et al. 1983; Panek and Fannon 1992; Pierce et al. 2009; Pratt et al. 1972; Simon and Deng 2009; Song et al. 2018). Only a few studies show that the UCS increases first and then decreases with size (Hawkins 1998; Masoumi et al. 2016; Nishimatsu et al. 1969; Quiñones et al. 2017; Zhai et al. 2020). The triaxial compression test conducts tests on rock specimens inside a pressure vessel. Since the vessel restricts the size of specimen that can be tested, size effect studies on the triaxial compressive strength (TCS) are significantly fewer than the studies

✉ Yun Zhao
cloudzhao0034@gmail.com

Brijes Mishra
Brijes.Mishra@utah.edu

Qingwen Shi
qs0003@mix.wvu.edu

Gaobo Zhao
gz00001@mix.wvu.edu

¹ West Virginia University, Morgantown, WV, USA

² The University of Utah, Salt Lake City, UT, USA

on UCS. Although studies of TCS are less available, most of them show that the TCS decreases as size increases (Li 2019; Medhurst and Brown 1998; Singh and Huck 1972), except for Masoumi et al. (2016) who reported that the TCS increases first and then decreases. In summary, research has more widely accepted that the compressive strength of rock decreases with the increase of size.

To explain the decreasing size effect of rock strength, previous researchers developed the statistical theory (Weibull 1939), fracture energy theory (Bažant 1984), and fractal theory (Carpinteri et al. 1995). The statistical theory assumes that a larger object is likely to contain more defects (or cracks), causing it to fail at a lower strength. Weibull (1939) completed the mathematical formulation of the statistical theory and proposed the statistical size effect model. The fracture energy theory originated from the Griffith theory that assumes material contains cracks and its failure initiates by the propagation of cracks. Griffith (1924) derived the critical stress required for crack propagation using a thermodynamic approach. Furthermore, Bažant (1984) related the material strength with material size and developed the size effect law based on non-linear fracture mechanics. The fractal theory assumes that the defects (or cracks) in a structure are self-similar; thus, the size of most dangerous defects is proportional to the structure size. Carpinteri (1994) pointed out that the dispersion of defect size on mechanical behavior becomes progressively less important for larger scales, whereas it represents the fundamental feature for smaller scales. Based on this assumption, Carpinteri et al. (1995) proposed the multifractal scaling law. In general, the three theories acknowledge that the cracks inside rock cause the decreasing size effect of rock strength.

However, in mechanics of material, material strength is size independent and failure criteria exclude size effect. To correlate the size effect of compressive strength, researchers have proposed different size effect models and then implemented them into failure criterion. Hoek and Brown (1980) proposed the most well-known size effect model to correlate the decreasing size effect of UCS. Medhurst and Brown (1998) later incorporated this size effect model into the Hoek–Brown failure. Furthermore, Song et al. (2018) considered the anisotropy of UCS and proposed an anisotropic size effect model, which was later incorporated into the Hoek–Brown failure criterion and Saeidi failure criterion by Li et al. (2021). In addition, Masoumi et al. (2017) put forward the unified size effect model and implemented it into the Hoek–Brown failure criteria to describe the ascending and then decreasing trend of compressive strength. Although these empirical failure criteria correlate well with the size effect of compressive strength, a theoretical failure criterion is necessary.

The objective of this research is to derive a theoretical failure criterion that can correlate the decreasing size effect of

compressive strength. The failure criterion assumes that the cracks inside rock cause the size effect. This research develops a numerical model of rock, in which it models cracks explicitly, to verify the proposed failure criterion. It collects experimental data in previous publications in order to check the applicability of the failure criterion. The research outcome will provide a new size-dependent failure criterion that can determine the compressive strength of rock at a large scale.

Formulation of the size-dependent Mohr-Coulomb failure criterion

The Griffith theory states that brittle material is filled with cracks, and a crack propagates when its maximum stress exceeds the molecular cohesive strength of material, and crack propagation is identified as material failure (Orowan 1949). Figure 1a shows a flat elliptical crack in a two-dimensional rock model, which is subjected to compressive stresses. σ_1 and σ_3 are the first and the third principal stresses; l is the crack length; r is the crack tip radius; and β is the orientation angle of the crack, which is defined as the angle between the direction of σ_1 and the normal to the crack long axis. McClintock and Walsh (1962) assumed that cracks are closed under compressive stress and there is friction effect along the crack surface. They derived the expression of the maximum stress at the crack tip as:

$$\sigma = \frac{1}{2}(l/r)^{1/2} [(\sigma_1 - \sigma_3)(\sin 2\beta - \mu \cos 2\beta) - \mu(\sigma_1 + \sigma_3)] \quad (1)$$

where μ is the friction coefficient of the crack surface. For later use, ϕ is the friction angle of the crack surface, $\mu = \tan \phi$. When the maximum stress reaches the molecular cohesive strength σ_{cr} , the crack starts to propagate. In such cases, the stress condition satisfies

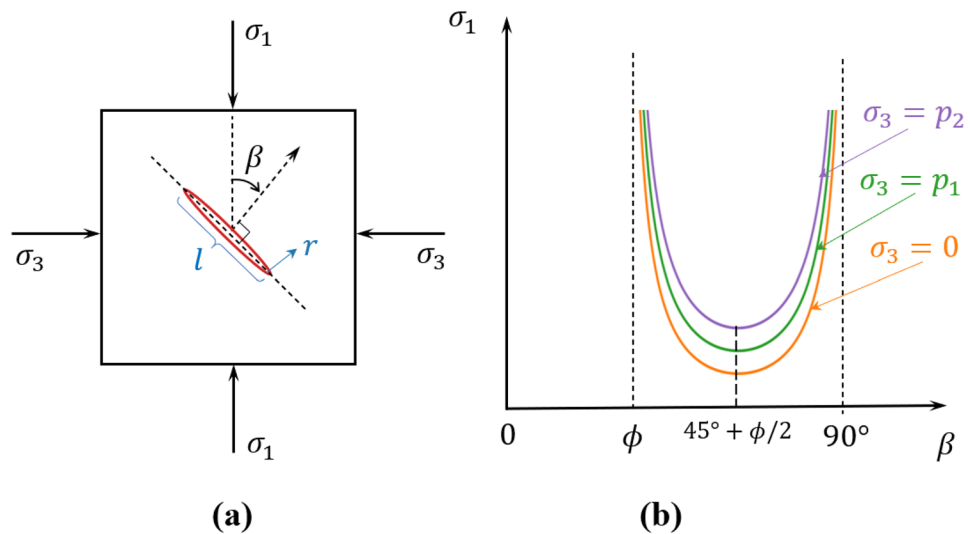
$$\sigma_1 = \frac{2\sigma_{cr}(l/r)^{-1/2} + \sigma_3(\mu - \mu \cos 2\beta + \sin 2\beta)}{-\mu - \mu \cos 2\beta + \sin 2\beta} \quad (2)$$

Since the crack propagation is identified as rock failure, Eq. (2) represents the stress condition of the rock failure. Figure 1b depicts the failure curve of the rock model caused by crack propagation. p_1 and p_2 represent different confining stresses ($p_2 > p_1 > 0$). The value of σ_1 tends to infinity as β equals ϕ or 90° , and, therefore, the crack propagation is not possible. The value of σ_1 is finite as β varies from ϕ to 90° and achieves minimum when $\beta = 45^\circ + \phi/2$. The minimum value of σ_1 is

$$\sigma_1^{min} = \frac{2\sigma_{cr}(l/r)^{-1/2}\cos \phi + \sigma_3(1 + \sin \phi)}{1 - \sin \phi} \quad (3)$$

It is necessary to consider that rock contains numerous cracks, and rock failure can occur at any crack. The Griffith

Fig. 1 **a** Two-dimensional rock model with single crack under compressive stresses; **b** failure curve of rock model caused by crack propagation



theory assumes that cracks have uniform orientation and position, the same crack tip radius, and that the interaction of cracks is negligible (Orowan 1949). This study accepts these assumptions. Furthermore, this study assumes that cracks have the same friction coefficient. As such, the crack length and orientation can determine the stress condition of any crack propagation, according to Eq. (2). Figure 2a shows the rock model with two cracks of different lengths and orientations. l and l_1 are the length of the long crack and the short crack, respectively. β is the orientation angle of the long crack. θ is the acute angle measured between the long axes of the two cracks; θ is positive when the measurement is in a clockwise direction from the long crack to the short crack, and θ is negative when measurement is in a counter-clockwise direction. Therefore, the orientation angle β_1 of the short crack is

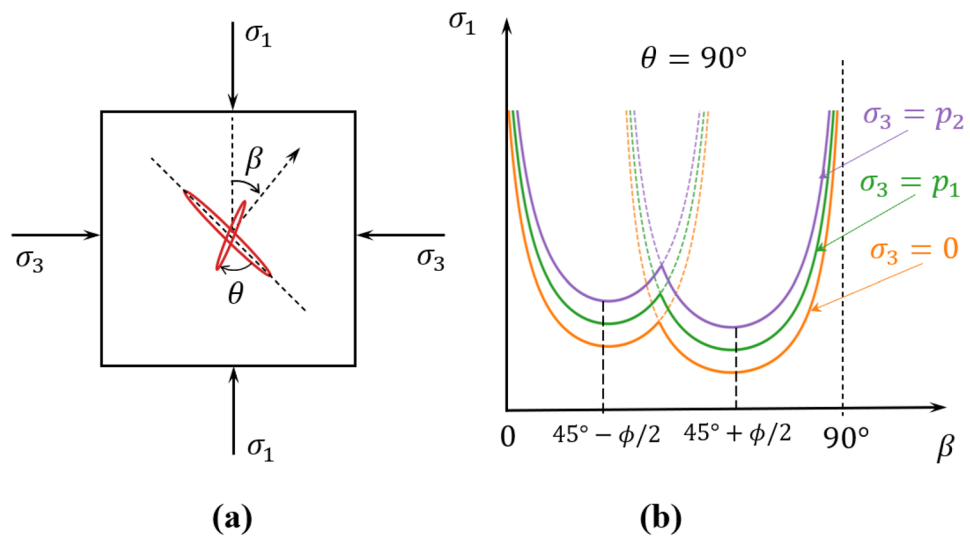
$$\beta_1 = \begin{cases} \min(\beta + \theta, 180^\circ - \beta - \theta), \theta \geq 0 \\ |\beta + \theta|, \theta < 0 \end{cases} \quad (4)$$

The stress condition of the short crack propagation is

$$\sigma_1 = \frac{2\sigma_{cr}(l_1/r)^{-1/2} + \sigma_3(\mu - \mu \cos 2\beta_1 + \sin 2\beta_1)}{-\mu - \mu \cos 2\beta_1 + \sin 2\beta_1} \quad (5)$$

Since the stress condition of the long crack propagation follows Eq. (3), the stress condition of the rock failure is given by the combination of Eqs. (3) and (5), and the overall compressive strength of rock is given by the lower stress of the equations. Figure 2b depicts the failure envelope of the rock model caused by crack propagation when $\theta = 90^\circ$. The value of σ_1 tends to infinity as β equals 0 or 90° . The value of σ_1 is finite as β varies from 0 to 90° and has two local minimum values when $\beta = 45^\circ + \phi/2$ and $\beta = 45^\circ - \phi/2$.

Fig. 2 **a** Two-dimensional rock model with two cracks under compressive stresses; **b** failure envelope of rock model caused by crack propagation when $\theta = 90^\circ$



The global minimum value of σ_1 is determined by the length of the long crack, which is the same as Eq. (3).

The above analysis can be applied to the case that rock contains numerous cracks. Figure 3a shows the rock model with twelve cracks of different lengths and orientation. β is the orientation angle of the longest crack of length l_{\max} . The stress condition of any crack propagation can be determined using Eqs. (3) and (5). Figure 3b depicts the failure envelope of the rock model caused by crack propagation. The overall compressive strength of rock is given by the lowest failure envelope of the individual failure curves. The value of σ_1 is finite as β varies from 0 to 90° and has several local minimum values. These local minimum values are different due to the different crack lengths. The length of the longest crack determines the global minimum value. It is important to note that, as the number of cracks increases, the failure envelope tends to be flat, and the overall compressive strength approximates to the global minimum value and becomes isotropic. Therefore, it is intuitive that the failure criterion of the rock containing numerous cracks is:

$$\sigma_1 = \frac{2\sigma_{cr}(l_{\max}/r)^{-1/2} \cos \phi + \sigma_3(1 + \sin \phi)}{1 - \sin \phi} \quad (6)$$

where l_{\max} is the length of the longest crack. Equation (6) demonstrates the relation between the compressive strength and the longest crack length. The compressive strength is lower if the rock contains longer cracks.

The analysis of the crack system in rock helps to determine the longest crack length l_{\max} . Bonnet et al. (2001) summarized that cracks exist on a wide range of lengths from micrometers to kilometers and their length distribution follows certain scaling laws. They compared different scaling laws and concluded that the power law provides the best description for the crack length distribution. If the crack

length distribution follows the power law, the crack number decreases with the increase of crack length as

$$N(l) = A \cdot l^{-a} \cdot D^2 \quad (7)$$

where $N(l)$ is the number of the cracks with a length in the range $[l, l + dl]$. A is a constant that determines the density of the crack system. a is a positive exponent that controls the relative proportion of cracks of different lengths, $a > 1$. D is the side length of the two-dimensional rock model. The crack length has the lower bound l_{\min} and the upper bound l_{\max} . The lower bound l_{\min} is finite since the smallest crack exists at the boundary of the smallest grains, while the upper bound l_{\max} can be infinite since the length distribution is not necessarily bonded to its upper bound (Itasca Consulting Group 2019). To find the longest crack length l_{\max} within the rock of size D , one must then use the cumulative crack length distribution, which defines the number of cracks with a length larger than a given value. Since there is no crack (less than one) with length longer than l_{\max} :

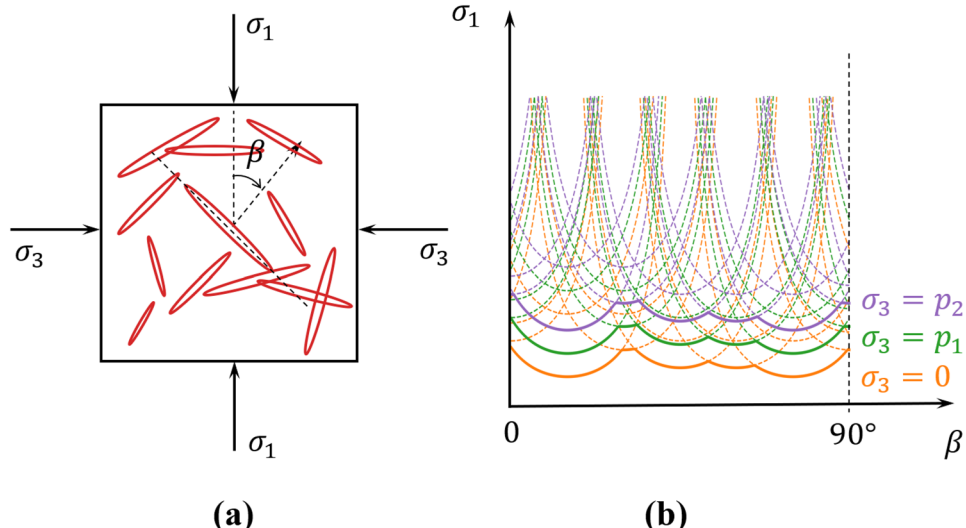
$$N(l > l_{\max}) = \int_{l_{\max}}^{\infty} N(l)dl = \frac{AD^2}{a-1} l_{\max}^{1-a} < 1 \quad (8)$$

Therefore,

$$l_{\max} = \left(\frac{A}{a-1} \right)^{\frac{1}{a-1}} D^{\frac{2}{a-1}} \quad (9)$$

Equation (9) demonstrates the relation between the longest crack length l_{\max} and the rock size D . l_{\max} increases as the rock size D increases, which means larger rock contains larger cracks. Figure 4 depicts the power law crack length distribution in a log-log diagram as a demonstration. The parameters A , a , D , l_{\min} , l_{\max} , and $N(l > l_{\max})$ are presented for further clarification.

Fig. 3 **a** Two-dimensional rock model with numerous cracks under compressive stresses; **b** failure envelope of rock model caused by crack propagation



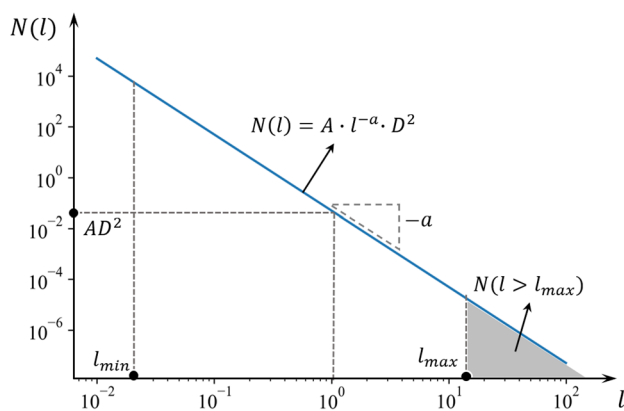


Fig. 4 Power-law crack length distribution in a log–log diagram

The relation between compressive strength and rock size is built by combining Eqs. (6) and (9):

$$\sigma_1 = \frac{2\sigma_{cr} r^{1/2} \left(\frac{A}{a-1}\right)^{-\frac{1}{2(a-1)}} D^{-\frac{1}{a-1}} \cos \phi + \sigma_3(1+\sin \phi)}{1-\sin \phi} = \frac{2c_0 D^{-k} \cos \phi + \sigma_3(1+\sin \phi)}{1-\sin \phi}$$

where $c_0 = \sigma_{cr} r^{1/2} \left(\frac{A}{a-1}\right)^{-\frac{1}{2(a-1)}}$ and $k = \frac{1}{a-1}$

(10)

where c_0 is the intrinsic cohesion of rock, k is the scaling constant, and ϕ is the friction angle of rock. Equation (10) demonstrates that the cohesion decreases as rock size increases while the friction angle is constant. Since the cohesion and friction angle of rock are measured through the laboratory test of the standard size (50 mm) specimens, Eq. (10) can be transformed into the normalized form:

$$\sigma_1 = \frac{2c_{50} \left(\frac{D}{50}\right)^{-k} \cos \phi + \sigma_3(1+\sin \phi)}{1-\sin \phi}, c_{50} = \sigma_{cr} r^{1/2} \left(\frac{2500A}{a-1}\right)^{-\frac{1}{2(a-1)}} \quad (11)$$

where c_{50} is the cohesion of the rock with the size of 50 mm. Equation (11) is named as the size-dependent Mohr–Coulomb failure criterion. In practice, it is difficult to characterize the crack system inside rock and calculate the cohesion c_{50} , the friction angle ϕ , and the scaling constant k directly. Instead, data fitting of experiment results can estimate c_{50} , ϕ , and k .

By setting $\sigma_3 = 0$, Eq. (11) becomes

$$\sigma_{cD} = \frac{2c_{50} \cos \phi}{1-\sin \phi} \left(\frac{D}{50}\right)^{-k} = \sigma_{c50} \left(\frac{D}{50}\right)^{-k} \quad (12)$$

where σ_{cD} is the UCS of the rock of size D , and σ_{c50} is the characteristic UCS of the rock with the size 50 mm. Figure 5 depicts the failure surfaces of the size-dependent failure criterion in the principal stress space. The two surfaces have the same c_{50} and ϕ but different k . The bold line represents the failure curve in the uniaxial compression state.

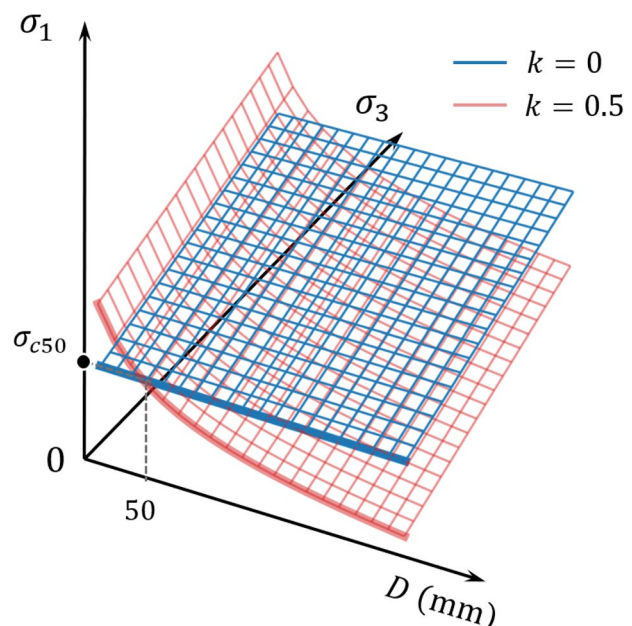


Fig. 5 Failure surfaces of size-dependent failure criterion in principal stress space

Validation of the proposed failure criterion based on numerical modeling

The development of the size-dependent Mohr–Coulomb failure criterion simplifies rock as consisting of matrix and cracks. The matrix is the base material that is size independent, while cracks are the structural features that cause the size effect of compressive strength. The failure criterion demonstrates that the crack length distribution parameters A and a influence the cohesion c_{50} and the scaling constant k . To validate the influence of the crack length distribution on the size effect of compressive strength, this research developed the bonded-particle model of rock consisting of matrix and cracks and tested it in the framework of PFC2D (Potyondy and Cundall 2004).

Bonded-particle model of rock

The bonded-particle model of rock mimics matrix using bonded particles and models cracks using discrete fractures. As shown in Fig. 6a, the model simulates the mechanical behavior of the matrix through the deformation and breakage of the bonds. The contact model of the bonds is the flat-joint model (Itasca Consulting Group 2019). The model generates cracks using the discrete fracture network (DFN) technique (Itasca Consulting Group 2019), given the geometric properties of cracks. As shown in Fig. 6b, cracks have the mechanical behavior of broken bonds, as the bonds that intersect the cracks inherit the same microparameters of matrix except

Fig. 6 Bonded-particle model of **a** matrix and **b** rock

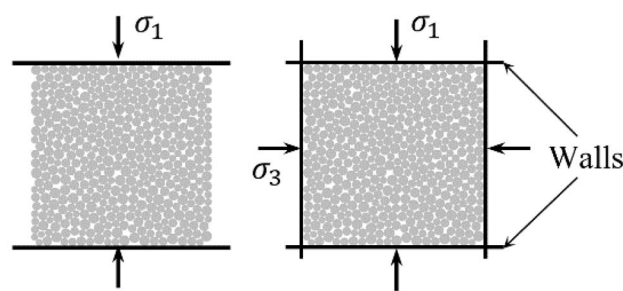
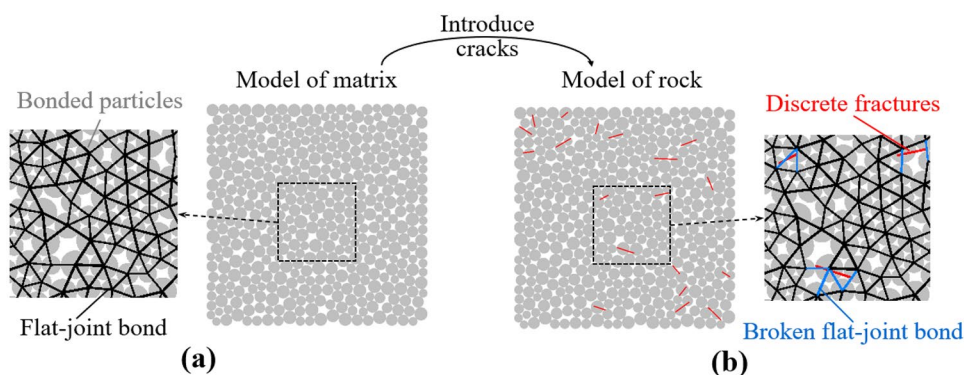


Fig. 7 Setup of uniaxial and triaxial compression test

that the tensile strength and cohesion are set as 0. Therefore, the microparameters of matrix and the geometric properties of cracks determine the compressive strength of the rock model. It is difficult to generate the rock model directly by calibrating the matrix and cracks at the same time. The rock model is developed in two steps. The first step is to calibrate the matrix model. The microparameters of matrix are adjusted so that its mechanical properties match those of real rock matrix and its UCS is independent of model size. The second step is to create the rock model by inserting the cracks into the matrix model. The model calibrates the geometric properties of cracks so that it presents the decreasing size effect of UCS.

This research conducted its model calibration through the uniaxial compression test. After calibration, it tested the model using the triaxial compression test to analyze the size effect of compressive strength. Figure 7 shows the setup of the uniaxial compression and the triaxial compression test. In the uniaxial compression test, a pair of frictionless grid walls simulates the loading platens. The triaxial compression test adds another pair of frictionless grid walls to apply a constant confining stress. Both the tests maintain the rate of loading at a level to ensure a quasi-static load on the model. The model genesis and compression test procedure follow “Material-Modeling Support for PFC [fistPkg6.6]” (Potyondy 2019).

Table 1 Microparameters of matrix

Parameter	Value
Common group:	
α, C_α, ρ_v [kg/m ³]	0.7, 1, 2558
$S_g, T_{SD}, \{D_{\{l,u\}}$ [mm], $\phi_v\}, D_{mult}$	0, 0, {1.0, 1.6, 1.0}, 1.0
Packing group:	
P_m [MPa], $\epsilon_P, \epsilon_{lim}, n_{lim}$	30, $1 \times 10^{-2}, 8 \times 10^{-3}, 2 \times 10^6$
C_p, n_c	1, 0.08
Flat-jointed material group:	
C_{MS}, g_i [mm], $\phi_B, \phi_G, (g_o)_{\{m,sd\}}$ [mm], $\{N_r, N_\alpha\}$	False, 0.15, 1, 0, {0, 0}, {2, 2} {0, 1}, 45, 3.6, 0.4
$\{C_\lambda, \lambda_v\}, E^*$ [GPa], κ^*, μ_f	{13.8, 0}, {37, 0}, 30
$(\sigma_c)_{\{m,sd\}}$ [MPa], $(c)_{\{m,sd\}}$ [MPa], ϕ_f [degrees]	
Linear material group:	
E_n^* [GPa], κ_n^*, μ_n	45, 3.6, 0.4

Model calibration

This research calibrated its matrix model at 50 mm so that the mechanical properties of the matrix model match those of Marcellus shale in our previous research. We selected that the Young's modulus and UCS of Marcellus shale are 38.79 GPa and 64.89 MPa. In fact, the other set of properties can be used as long as they are reasonable for rock. The value of these microparameters was obtained through a trial-and-error approach so that the Young's modulus and UCS of the matrix model are 38.79 GPa and 64.89 MPa, respectively. The calibration procedure in detail has been explained in the reference (Potyondy 2019).

Table 1 lists the microparameters of the matrix model after calibration. The common group defines the parameters in the particle genesis procedure, including local-damping factor α , density code C_α , density value ρ_v , grain-shape code S_g , size-distribution type T_{SD} , diameter range $D_{\{l,u\}}$ (lower and upper), volume fraction ϕ_v , and diameter multiplier D_{mult} ; the packing group defines the parameters in the particle packing procedure, including material pressure P_m , pressure tolerance ϵ_P , equilibrium-ratio limit ϵ_{lim} , step limit

n_{\lim} , packing-procedure code C_P , and grain-cloud porosity n_c ; the flat-jointed material group defines the parameters for flat-joint contacts, including microstructure-tracking flag C_{MS} , installation gap g_i , bonded fraction ϕ_B , gapped fraction ϕ_G , initial surface-gap distribution $(g_o)_{\{m,sd\}}$, elements in radial direction N_r and circumferential direction N_α , radius multiplier code C_λ and value λ_v , effective modulus E^* , stiffness ratio κ^* , friction coefficient μ_f , tensile-strength distribution $(\sigma_c)_{\{m,sd\}}$, cohesion distribution $(c)_{\{m,sd\}}$, and friction angle ϕ_f ; the linear material group defines the parameters for particle-particle contacts during packing and that may form subsequent to material finalization, including effective modulus E_n^* , stiffness ratio κ_n^* , and friction coefficient μ_n . Readers who are interested in these parameters could find the specific definition and meaning in Potyondy (2019).

This research regenerated the matrix model to the sizes of 25, 75, 100, 125, 150, and 200 mm with the same micro-parameters. Figure 8a shows the matrix model at sizes of 25, 50, and 75 mm as a demonstration. Figure 8b compares the stress-strain curves of the matrix models at sizes from 25 to 200 mm. The figure shows that the value of Young's modulus and UCS varies little as the model size increases. Therefore, the calibrated matrix model's mechanical properties match those of real rock matrix and its UCS is independent of model size.

This research calibrated the rock model by adjusting the geometric properties of cracks so that the rock model presents the decreasing size effect of UCS. Table 2 lists the geometric properties of cracks. The position and orientation of cracks follow the uniform distribution. The length of the cracks follows the power law distribution. The value of l_{\min} was set as the smallest size of particles, since the smallest crack exists at the boundary of the smallest particles. Figure 9a shows the rock model at sizes of 25, 50, and 75 mm as a demonstration. Figure 9b compares the

Table 2 Geometric properties of cracks

Parameter	Position	Orientation	Power-law length distribution		
			A	a	$l_{\min}[\text{mm}]$
Value	Uniform	Uniform	0.05	3	1

stress-strain curves of the rock models at sizes from 25 to 200 mm. It shows that the introduction of cracks decreases the Young's modulus and UCS. Furthermore, the value of Young's modulus and UCS decreases as the model size increases in the general case. The decreasing trend is not strictly applied in the cases of 25, 50, and 200 mm. The cause of this anomaly is that the packing arrangement of matrix and crack varies greatly with the change in the model size, and the packing arrangement influences the mechanical behavior. To avoid this anomaly, this research will use the average value of 10 realizations (using the same parameters) to analyze the size effect of compressive strength.

Size effect on the compressive strength of the rock model

To eliminate the influence of the packing arrangement, this research created 10 realizations for each model size by varying the random seed (Potyondy 2019). Figure 10 shows the 7 different-sized models and their 10 realizations for both matrix and rock. These 140 models are tested in the uniaxial compression and the triaxial compression with the confining stress $\sigma_3 = 3, 5$, and 10 MPa.

Figure 11 presents the compressive strength of the models of matrix and rock. Each dot represents the model strength with the specific size, confining stress, and random seed. The

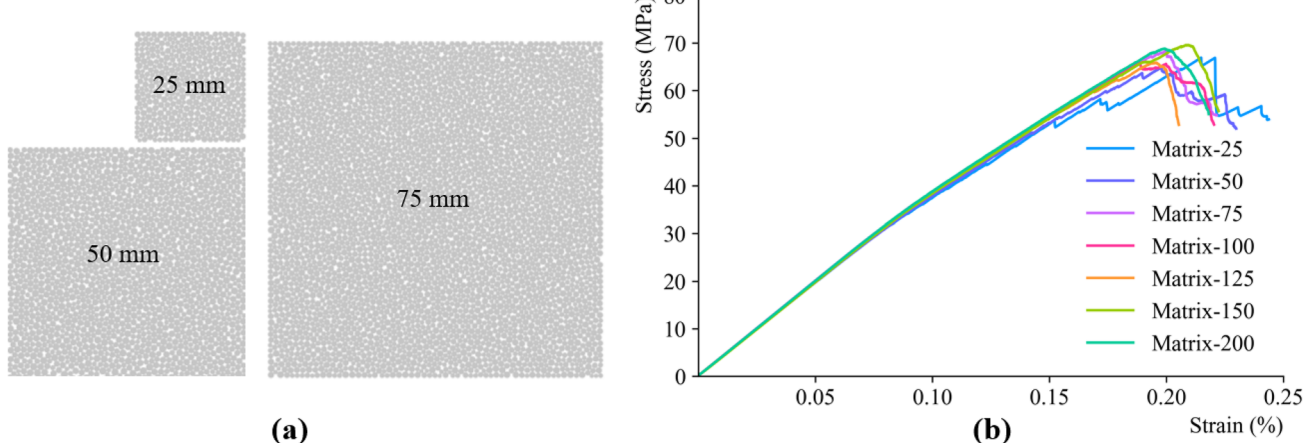


Fig. 8 **a** Matrix models of size 25, 50, and 75 mm; **b** stress-strain curves of matrix models at sizes from 25 to 200 mm

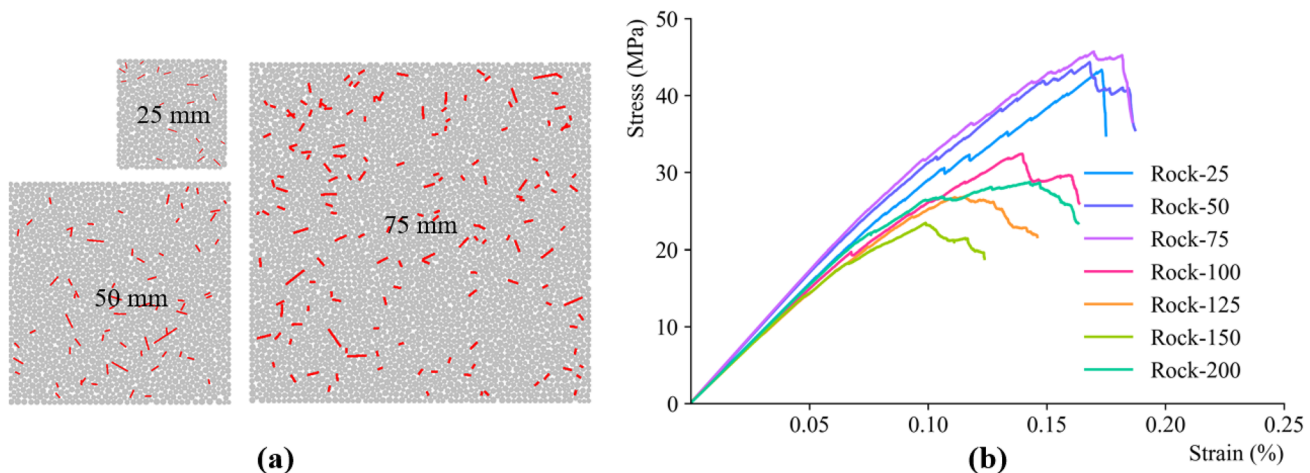


Fig. 9 **a** Rock models of size 25, 50, and 75 mm; **b** stress–strain curves of rock models at sizes from 25 to 200 mm

change of random seed causes the variation of the model strength. The compressive strength variation decreases with the increase of model size but is little affected by the confining stress. The compressive strength variation of rock is more prominent than that of matrix. This research then used the average compressive strength of the 10 realizations to compare the size effect of compressive strength. Each line represents the change of the average strength with different model sizes in different confining stresses. The result shows that the compressive strength of matrix and rock increases as the confining stress increases. The compressive strength of matrix model varies little with the increase of model size, while the compressive strength of rock model decreases significantly. Therefore, the compressive strength of matrix is size independent, and the introduction of cracks causes the size effect on the compressive strength of rock.

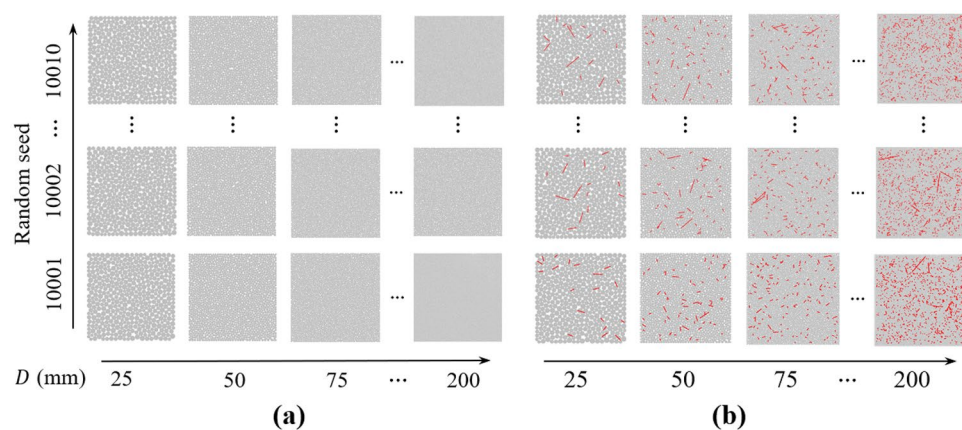
Figure 12 shows the fitting result of the compressive strength of matrix and rock using the size-dependent Mohr–Coulomb failure criterion. Each dot represents the average strength of the 10 realizations, and the wireframe

represents the best fitting failure surface. For the matrix model, the cohesion c_{50} and friction angle ϕ are 17.25 MPa and 37.36°, respectively, the scaling constant is $k = 0.02 \cong 0$, and the coefficient of determination is $R^2 = 0.97$. For the model of rock, the cohesion c_{50} and friction angle ϕ are 11.76 MPa and 30.44°, respectively, the scaling constant is $k = 0.24$, and the coefficient of determination is $R^2 = 0.95$. Therefore, the proposed failure criterion fits well with the compressive strength of matrix and rock. The introduction of cracks decreases c_{50} and ϕ and increases k .

Parametric analysis of the influence of the crack length distribution

The size-dependent Mohr–Coulomb failure criterion demonstrates that the crack length distribution parameters A and a influence the cohesion c_{50} and the scaling constant k . This influence can be verified from the triaxial compression test of the rock models with different A and a . However, it is time consuming to run the triaxial compression test on a large

Fig. 10 Schematic view of different-size models and their 10 realizations: **a** matrix model and **b** rock model



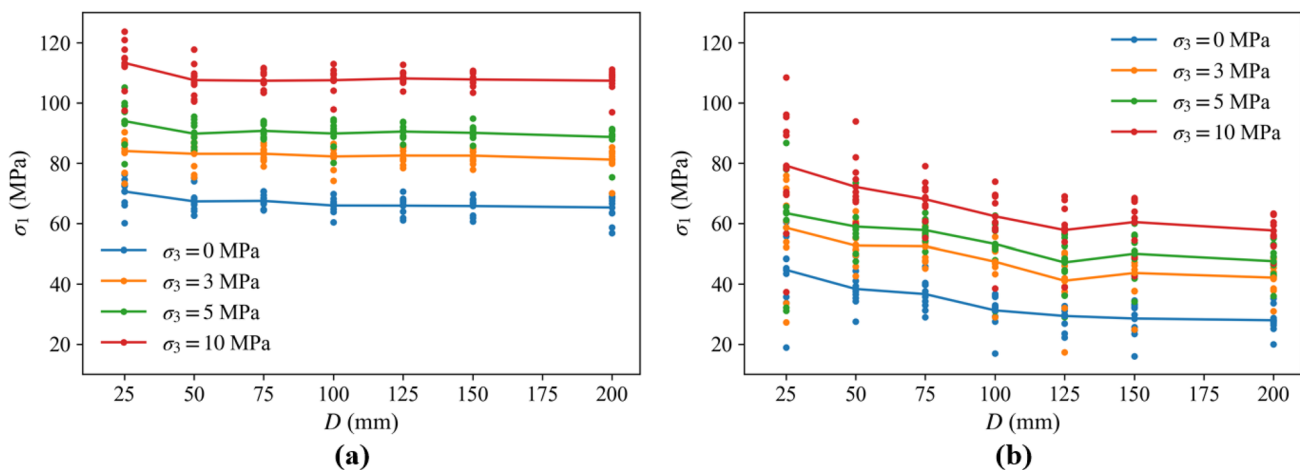


Fig. 11 Compressive strength results of models: **a** matrix model and **b** rock model

amount of rock models. To reduce the modeling time, this research tested these models only in the uniaxial compression test. It analyzed the influence on σ_{c50} instead of on c_{50} , since $\sigma_{c50} = 2c_{50}\cos\phi/(1 - \sin\phi)$ and ϕ is a constant regardless the change of A and a .

According to the proposed failure criterion, the increase of A decreases σ_{c50} but has no influence on k . Figure 13 presents the influence of A on the crack distribution in the model of size 100 mm and random seed 10,001. When $A = 0.03$, the range of crack length is from 1 to 10 mm. When $A = 0.05$, the crack density increases, and the model is more likely to contain large cracks; therefore, there is a

crack with a length over 25 mm. When $A = 0.07$, the crack density continues to increase, introducing more cracks. Figure 14 shows the influence of A on the size effect of UCS. Each dot represents the average strength of the 10 realizations, and each line represents the best-fitting failure curve. The coefficients of determination R^2 are equal to or greater than 0.90. When A increases from 0.03 to 0.07, σ_{c50} decreases significantly from 47.50 to 30.28 MPa, but k varies little from 0.22 to 0.25. This result corresponds well with the previous statement about the influence of A .

According to the proposed failure criterion, the increase of a decreases k but increases σ_{c50} . Figure 15 shows the

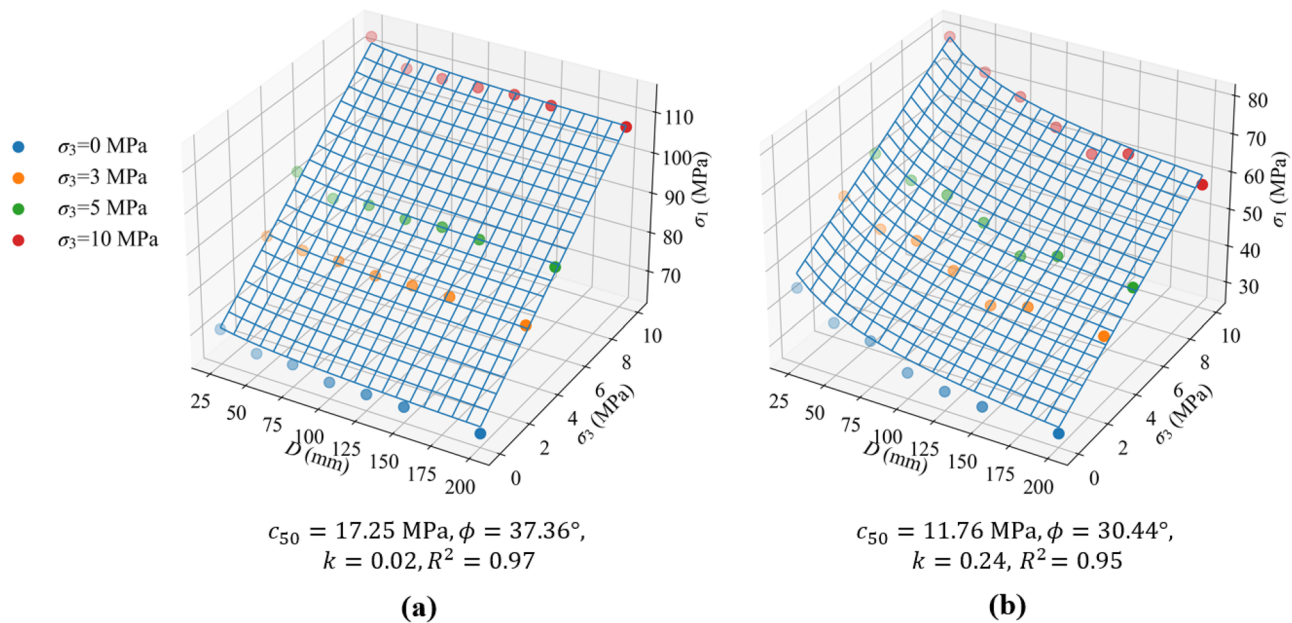
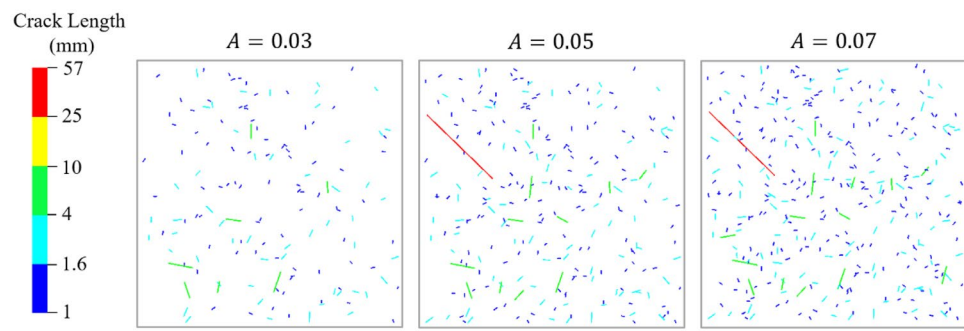


Fig. 12 Fitting result of the compressive strength of **a** matrix model and **b** rock model

Fig. 13 Influence of A on crack distribution in model of size 100 mm and random seed 10,001



influence of a on the crack distribution in the model of size 100 mm and random seed 10,001. When $a = 2$, the range of crack length is from 1 to 57 mm. When $a = 3$, the proportion of large cracks decreases while the proportion of small crack increases. When $a = 4$, there is no crack with a length over 25 mm. When $a = 5$, the longest crack length is below 10 mm. When a tends to ∞ , all the cracks have the same length of 1 mm. Figure 16 shows the influence of a on the size effect of UCS. Each dot represents the average strength of the 10 realizations, and each line represents the best-fitting failure curve. The coefficient of determination R^2 decreases from 0.99 to 0.89 as a increases from 2 to 5. The R^2 equals 0.64 when a tends to ∞ and still shows applicability. σ_{c50} increases from 19.04 to 48.83 MPa as a increases from 2 to 5, and the increase rate declines. As a tends to ∞ , the value of σ_{c50} is a finite constant 51.41 MPa. As for the influence of a on k , when $a = 2, 3, 4, 5$, and ∞ , the theoretical results of k should be 1, 0.5, 0.25, 0.13, and 0. However, the modeling results of k are 1.10, 0.24, 0.10, 0.09, and 0.03. The theoretical and numerical results are close when $a = 2, 5$, and ∞ but are different when $a = 3$ and 4. Although there is difference, k decreases as a increases and k approaches 0 as a tends to ∞ in a general case. This result corresponds well with previous statements about the influence of a .

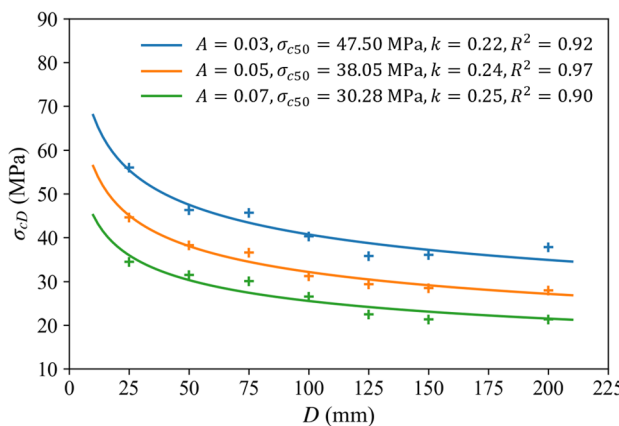


Fig. 14 Influence of A on size effect of UCS

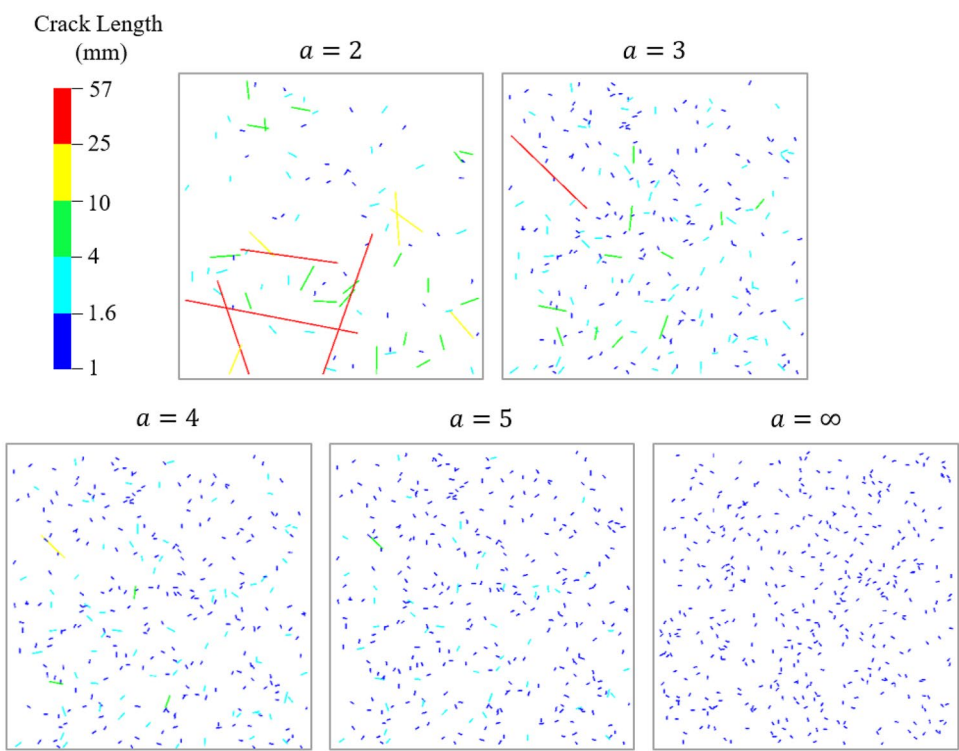
Application of the proposed failure criterion to experimental data

The bonded-particle model of rock verified that cracks cause the size effect of compressive strength, and the crack length distribution affects the size effect of compressive strength according to the size-dependent Mohr–Coulomb failure criterion. This section applied the proposed failure criterion to the experimental data of previous size effect research. It is important to note that this study focuses on the effect of size, and the term “size” refers to the diameter of a cylinder or the width of a rectangular prism. The experimental data processing neglected the influence of shape and slenderness ratio, although the rock specimens have the shapes of cylinders and rectangular prisms and different slenderness ratios.

Experimental data of UCS

Figure 17 plots the experimental data that present the decreasing size effect of UCS. Each dot represents the UCS of the specific rock with the specific size, and each line represents the change of UCS with different sizes of the specific rock. This picture contains 30 datasets from 19 different publications; Table 3 lists the legend. The range of publication year for these studies is from 1962 to 2021. The rock types include marble, iron ore, granite, coal, diorite, siderite, gypsum, diabase, basalt, quartzite, cement mortar, slate, and sandstone. Therefore, this compilation considers all types of rock, including igneous rock, metamorphic rock, sedimentary rock, and artificial rock. The size range of the rock specimens is from 12.5 to 1828.8 mm. This study retrieves most of this data (Baecher and Einstein 1981; Bieniawski 1968; Gonzatti et al. 2014; Herget and Unrug 1976; Hoskins and Horino 1969; Jackson and Lau 1990; Kong et al. 2021; Li 2019; Lundborg 1967; Mogi 1962; Pierce et al. 2009; Pratt et al. 1972; Song et al. 2018) from the publications directly; it calculated the rest (Abou-Sayed and Brechtel 1976; Darlington et al. 2011; Jahns 1966; Natau et al. 1983; Panek and Fannon 1992; Simon and Deng 2009) based on the provided fit equation or estimated it from the original

Fig. 15 Influence of a on crack distribution in model of size 100 mm and random seed 10,001



picture. It is worthy to note that Song et al. (2018) and Li (2019) tested coal and slate specimens respectively in six directions with the orientation angles of 0° , 15° , 30° , 45° , 60° , and 90° . Since most data are in the size range of 0 to 200 mm, the figure upscales this area for clear presentation. Table 3 shows the fitting result of the experimental data of UCS. The value of σ_{c50} varies from 9.65 to 319.42 MPa. The value of k varies from 0.08 to 0.77, and most are below 0.5. The coefficients of determination R^2 for most datasets are over 0.9, showing that the size-dependent Coulomb criterion fits the experimental data of UCS well.

Following the work of Hoek and Brown (1980), this study reduces the UCS data to dimensionless forms by dividing the individual values σ_{cD} by the value σ_{c50} . Figure 18 shows the influence of specimen size on the σ_{cD}/σ_{c50} in the dimensionless form. Each point represents the value of σ_{cD}/σ_{c50} for the specific rock with a specific size, and the orange line represents the overall best-fitting line with $k = 0.36$. The model fits well with the data as $R^2 = 0.76$. The dashed lines with $k = 0.08$ and 0.77 present the lower bound and the upper bound of k . The blue solid line with $k = 0.18$ represents the fitting result in Hoek and Brown (1980). The

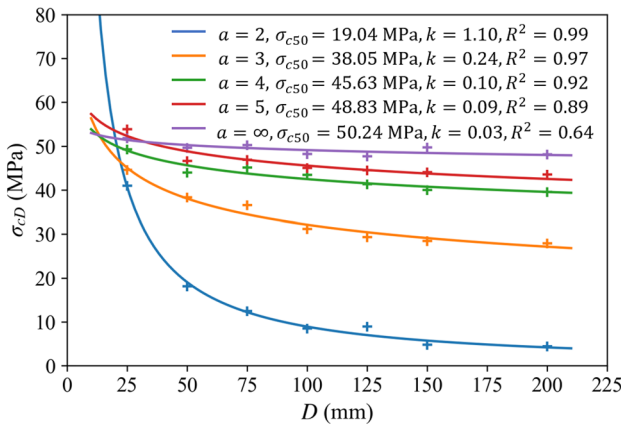


Fig. 16 Influence of a on size effect of UCS

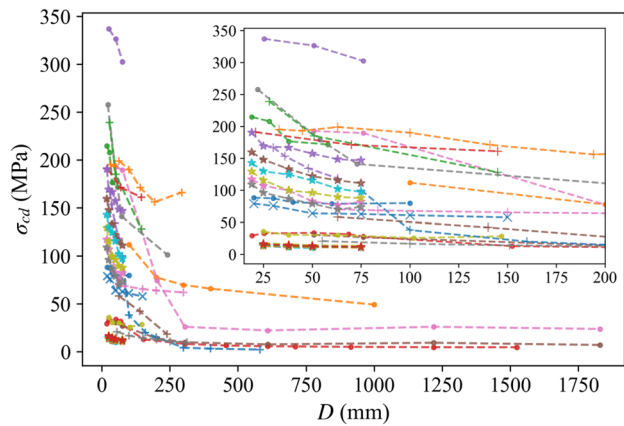
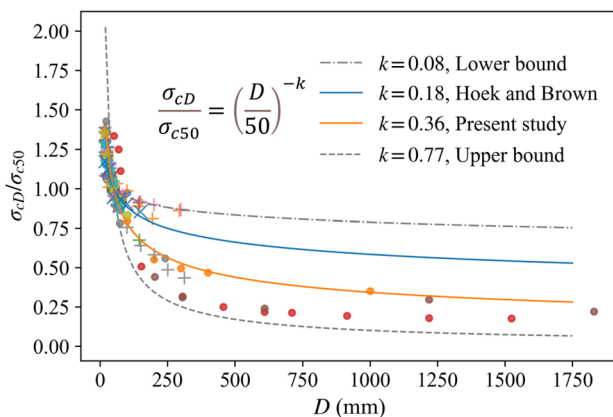


Fig. 17 Experimental data showing decreasing size effect of UCS

Table 3 The fitting result of experimental data of UCS

Line type	Publications	σ_{c50} (MPa)	k	R^2
—●—	Yamaguchi marble, Mogi (1962)	81.99	0.08	0.77
—○—	Iron ore, Jahns (1966)	140.54	0.38	0.97
—●—	Granite, Lundborg (1967)	174.67	0.23	0.88
—●—	Coal, Bieniawski (1968)	25.23	0.42	0.82
—●—	Salida granite, Hoskins and Horino (1969)	319.42	0.09	0.86
—●—	Quartz Diorite, Pratt et al. (1972)	30.95	0.51	0.95
—●—	Graddiorite, Pratt et al. (1972)	214.39	0.77	0.93
—●—	Sound siderite, Herget and Unrug (1976)	180.78	0.42	0.98
—●—	Quartz diorite, Abou-Sayed and Brechtel (1976)	30.78	0.15	0.76
—●—	Gypsum, Baecher and Einstein (1981)	9.65	0.44	0.97
—●—	Grey granite, Jackson and Lau (1990)	193.15	0.10	0.75
—●—	Metadiabase, Panek and Fannon (1992)	189.88	0.38	1.00
—●—	Ophitic basalt, Panek and Fannon (1992)	176.67	0.09	1.00
—●—	Intact rock, Simon and Deng (2009)	131.76	0.46	1.00
—●—	Quartzite, Pierce, Gaida, and DeGagne (2009)	69.78	0.68	0.89
—●—	Cement mortat, Darlington, Ranjith, and Choi (2011)	71.31	0.08	1.00
—●—	Coal, Gonzatti et al. (2014)	21.88	0.43	0.99
—●—	Coal at 0°, Song et al. (2018)	14.69	0.25	0.98
—●—	Coal at 30°, Song et al. (2018)	12.23	0.24	0.98
—●—	Coal at 45°, Song et al. (2018)	11.31	0.21	0.98
—●—	Coal at 60°, Song et al. (2018)	11.25	0.22	0.98
—●—	Coal at 75°, Song et al. (2018)	12.64	0.25	0.99
—●—	Coal at 90°, Song et al. (2018)	13.12	0.28	0.98
—●—	Slate at 0°, Li (2019)	156.33	0.18	0.93
—●—	Slate at 30°, Li (2019)	122.90	0.27	1.00
—●—	Slate at 45°, Li (2019)	87.11	0.31	0.93
—●—	Slate at 60°, Li (2019)	79.06	0.31	0.96
—●—	Slate at 75°, Li (2019)	95.64	0.29	0.98
—●—	Slate at 90°, Li (2019)	111.20	0.26	0.95
—●—	Red sandstone, Kong, Liu, and Lu (2021)	67.52	0.17	0.94

value of k in the present study is different from that in Hoek and Brown's work; the cause of this difference is that this research includes a higher number of datasets.

**Fig. 18** Influence of specimen size on the UCS of rock in the dimensionless form

Experimental data of TCS

Figure 19 plots the experimental data showing the decreasing size effect of TCS. Each dot represents the TCS of specimens of a specific size under a specific confining stress, and the wireframe represents the best-fitting failure surface. As stated previously, this study retrieved the data of slate directly from the previous paper and calculated the data of coal based on the provided fit equation. Singh and Huck (1972) showed the decreasing size effect of the TCS of Charcoal black granite; however, their experiment only tested the granite in two sizes. Therefore, this study does not present their experimental data here. The coefficient of determination R^2 for all the data is over 0.9, showing that the size-dependent Coulomb criterion fits the TCS well.

Table 4 lists the fitting result of the experimental data of TCS. The value of σ_{c50} is calculated according to $\sigma_{c50} = 2c_{50}\cos\phi/(1 - \sin\phi)$. The σ_{c50} and k in Table 4 are different from those in Table 3. The difference is small for

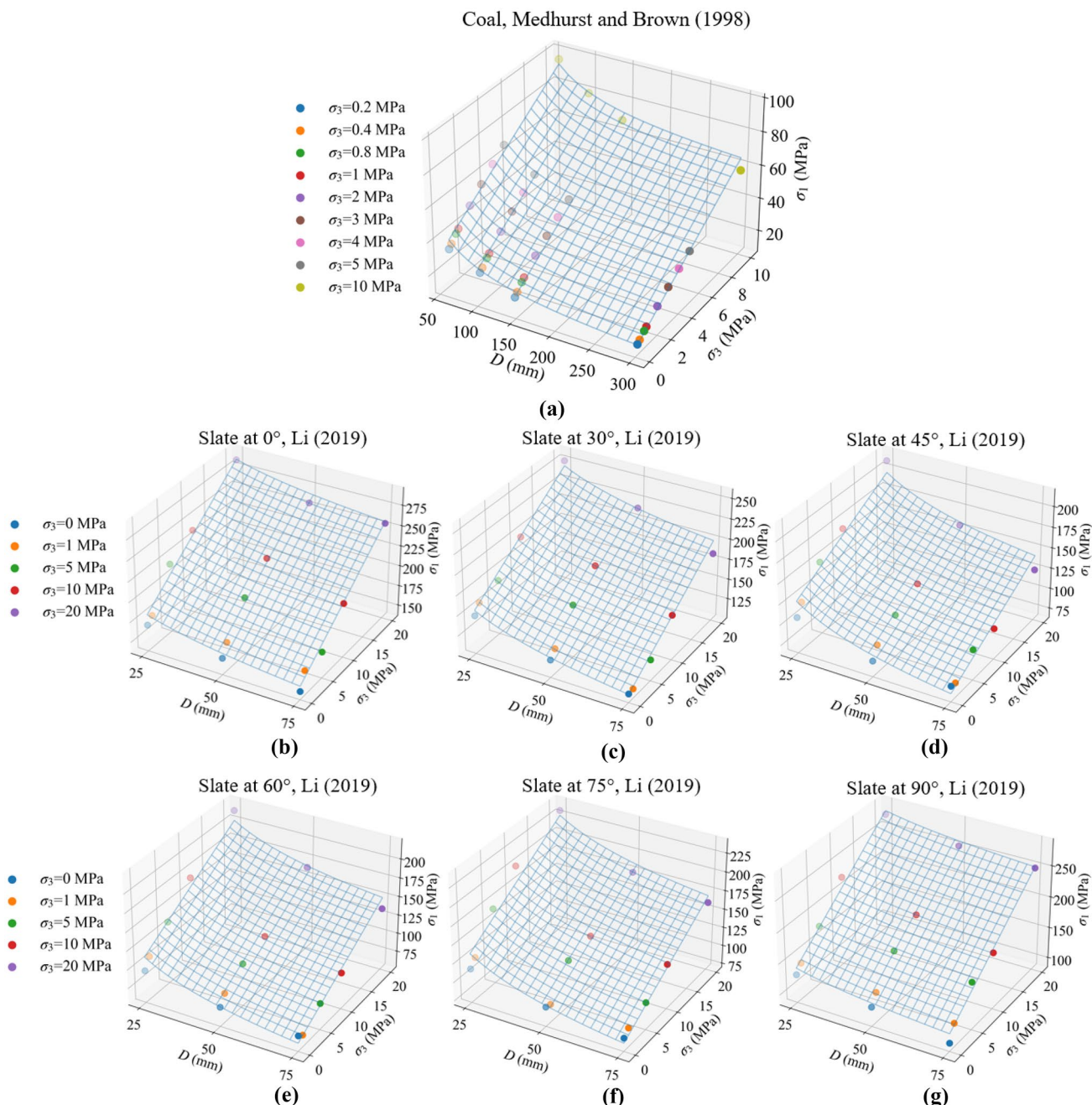


Fig. 19 Experimental data showing decreasing size effect of TCS and best-fitting failure surface

σ_{c50} . The difference is significant for the k in the datasets of Slate at 45°, 60°, and 75°. The reason is that the data fitting of the TCS includes more data. Although the value of k can be estimated from the UCS of different-sized rock specimens, it requires adjustment to achieve the least sum of squares of error to fit the TCS. It is interesting to note that the value of k varies as the orientation angle of slate changes, indicating that the size effect of slate strength is affected by its anisotropy.

Discussion

This research theoretically derived the size-dependent Mohr–Coulomb failure criterion based on the Griffith theory, developed the bonded-particle model of rock to validate the failure criterion, and collected previous experimental data to check the applicability of the failure criterion. Moreover, there is experimental evidence that supports the size-dependent Mohr–Coulomb failure criterion. Tani (2001) investigated the

Table 4 Fitting result of experimental data of TCS

Publications	c_{50} (MPa)	$\phi(^{\circ})$	σ_{c50} (MPa)	k	R^2
Coal, Medhurst and Brown (1998)	9.78	43.48	45.51	0.75	0.97
Slate at 0°, Li (2019)	35.71	42.76	163.32	0.16	0.94
Slate at 30°, Li (2019)	29.31	39.71	124.88	0.31	0.95
Slate at 45°, Li (2019)	23.98	33.72	89.67	0.50	0.92
Slate at 60°, Li (2019)	18.93	38.95	79.29	0.53	0.95
Slate at 75°, Li (2019)	23.05	39.61	97.99	0.47	0.92
Slate at 90°, Li (2019)	23.13	48.49	122.07	0.20	0.97

size effect of mudstone using the triaxial compression test and found the cohesion decreases as the specimen size increases following $c_D = c_{50}(D/50)^{-k}$, with $k = 0.5$. Kong et al. (2021) studied the size effect of sandstone using the direct shear test and determined $k = 0.221$. Their works show that the friction angle is independent of rock size. In addition, numerous empirical studies have verified the proposed failure criterion in the uniaxial compression state (the size effect model of UCS). Mogi (1962) first proposed the size effect model based on data fitting. Hoek and Brown (1980) analyzed the experimental data in publications and found the value of k is 0.18 for most rocks. Yoshinaka et al. (2008) summarized more experimental data and concluded that k ranges from 0.1 to 0.3 for hard rock and from 0.3 to 0.9 for soft rock.

The proposed failure criterion contains three parameters: the cohesion c_{50} , the friction angle ϕ , and the scaling exponent k . c_{50} and ϕ can be estimated from the TCS of standard size rock specimens, while k can be estimated from the UCS of different-sized rock specimens. Therefore, one can determine the parameters of the proposed failure criterion based on the uniaxial compression test of different-sized specimens and the triaxial compression test of standard-size specimens. However, including more TCS data of different-sized specimens can improve the accuracy of the parameters. The determined failure criterion can then predict the TCS of different-sized specimens at different confining stresses.

The data fitting of anisotropic rock shows that the value of k varies as the orientation angle of rock changes, indicating that the size effect of compressive strength is affected by its anisotropy. However, the proposed failure criterion does not consider the strength anisotropy that is highly prominent in some rocks. We are working on this problem and plan to incorporate the strength anisotropy into the proposed failure criterion.

Conclusion

- (1) The size-dependent Mohr–Coulomb failure criterion contains three parameters: the cohesion, the friction angle, and the scaling exponent. The cohesion decreases as rock size increases, while the friction angle is inde-

pendent of rock size. This failure criterion demonstrates that the cracks inside rock cause the size effect and the crack length distribution affects the size effect.

- (2) The bonded-particle model of rock verified that cracks cause the size effect of the compressive strength. The parametric analysis verified the influence of crack length distribution on the cohesion c_{50} and the scaling exponent k . The increase of A decreases c_{50} but has little influence on k ; the increase of a increases c_{50} and decreases k .
- (3) The proposed failure criterion fits well with the experimental data of UCS and TCS. The fitting result shows k varies from 0.08 to 0.77. The fitting result of UCS in the dimensionless form shows $k = 0.36$ for all data, which is different from $k = 0.18$ in Hoek and Brown (1980).

Data Availability The data that support the findings of this study are available in Zhao (2022).

Declarations

Competing interests The authors declare no competing interests.

References

- Abou-Sayed AS, Brechtel CE (1976) Experimental investigation of the effects of size on the uniaxial compressive strength of cedar city quartz diorite. In: The 17th US Symposium on Rock Mechanics (USRMS)
- Baecher GB, Einstein HH (1981) Size effect in rock testing. *Geophys Res Lett* 8:671–674
- Bažant ZP (1984) Size effect in blunt fracture: concrete, rock, metal. *J Eng Mech* 110:518–535
- Bieniawski ZT (1968) Propagation of brittle fracture in rock. In: The 10th US Symposium on Rock Mechanics (USRMS)
- Bonnet E, Bour O, Odling NE, Davy P, Main I, Cowie P, Berkowitz B (2001) Scaling of fracture systems in geological media. *Rev Geophys* 39:347–383
- Carpinteri A (1994) Fractal nature of material microstructure and size effects on apparent mechanical properties. *Mech Mater* 18:89–101
- Carpinteri A, Chiaia B, Ferro G (1995) Size effects on nominal tensile strength of concrete structures: multifractality of material ligaments and dimensional transition from order to disorder. *Mater Struct* 28:311

- Darlington WJ, Ranjith PG, Choi SK (2011) The effect of specimen size on strength and other properties in laboratory testing of rock and rock-like cementitious brittle materials. *Rock Mech Rock Eng* 44:513–529
- Gonzatti C, Zorzi L, Agostini IM, Fiorentini JA, Viero AP, Philipp RP (2014) In situ strength of coal bed based on the size effect study on the uniaxial compressive strength. *Int J Min Sci Technol* 24:747–754
- Griffith A (1924) The theory of rupture. First Int Cong Appl Mech, a221
- Hawkins AB (1998) Aspects of rock strength. *Bull Eng Geol Environ* 57:17–30
- Herget G, Unrug K (1976) In situ rock strength from triaxial testing. *Int J Rock Mech Min Sci Geomech Abstr* 13(11):299–302
- Hoek E, Brown ET (1980) Underground excavations in rock, 1st ed. CRC Press, pp 155–156
- Hoskins JR, Horino FG (1969) Influence of spherical head size and specimen diameters on the uniaxial compressive strength of rocks. [16 refs]. United States
- Itasca Consulting Group (2019) PFC 6.0 documentation
- Jackson R, Lau J (1990) The effect of specimen size on the laboratory mechanical properties of Lac du Bonnet grey granite. Proceedings of the first International Workshop on Scale Effects in Rock Masses, pp 165–174
- Jahns H (1966) Measuring the strength of rock in situ at an increasing scale. Paper presented at the 1st ISRM Congress, Lisbon, Portugal
- Kong X, Liu Q, Lu H (2021) Effects of rock specimen size on mechanical properties in laboratory testing. *J Geotech Geoenvir Eng* 147:04021013
- Li K (2019) Size effect and anisotropy in transversely isotropic rocks. Doctor's thesis. Hong Kong Polytechnic University
- Li K, Yin Z-Y, Han D, Fan X, Cao R, Lin H (2021) Size effect and anisotropy in a transversely isotropic rock under compressive conditions. *Rock Mech Rock Eng* 54(9):4639–4662
- Lundborg N (1967) The strength-size relation of granite. *Int J Rock Mech Min Sci Geomech Abstr* 4(3):269–272
- Masoumi H, Roshan H, Hagan PC (2017) Size-dependent Hoek-Brown failure criterion. *Int J Geomech* 17(2):04016048
- Masoumi H, Saydam S, Hagan PC (2016) Unified size-effect law for intact rock. *Int J Geomech* 16:1–15
- McClintock FA, Walsh J (1962) Friction on Griffith's cracks in rock under pressure. US National Congress on Applied Mechanics, pp 1015–1021
- Medhurst TP, Brown ET (1998) A study of the mechanical behaviour of coal for pillar design. *Int J Rock Mech Min Sci* 35:1087–1105
- Mogi K (1962) The influence of the dimensions of specimens on the fracture strength of rocks: comparison between the strength of rock specimens and that of the earth's crust. *Bull. Earthq. Res. Institute. Univ Tokyo* 40:175–185
- Natau OP, Frohlich BO, Mutschler TO (1983) Recent developments of the large-scale triaxial test. In: 5th ISRM Congress, pp 65–74
- Nishimatsu Y, Yamaguchi U, Motosugi K, Morita M (1969) The size effect and experimental error of the strength of rocks. *J Min Mat Proc Inst Jpn* 18:1019–1025
- Orowan E (1949) Fracture and strength of solids. *Rep Prog Phys* 12:185
- Panek LA, Fannon TA (1992) Size and shape effects in point load tests of irregular rock fragments. *Rock Mech Rock Eng* 25:109–140
- Peng SS (2015) Topical areas of research needs in ground control—a state of the art review on coal mine ground control. *Int J Min Sci Technol* 25:1–6
- Pierce M, Gaida M, DeGagne D (2009) Estimation of rock block strength. In: RockEng09 (Proceedings, 3rd CANUS Rock Mechanics Symposium, Toronto)
- Potyondy DO (2019) Material-modeling support in PFC [fistpkg6.6]. Itasca Consult. Group, Inc., Minneapolis, Minnesota, Tech. Memo. ICG7766-L (December 11, 2019)
- Potyondy DO, Cundall PA (2004) A bonded-particle model for rock. *Int J Rock Mech Min Sci* 41:1329–1364
- Pratt HR, Black AD, Brown WS, Brace WF (1972) The effect of specimen size on the mechanical properties of unjointed diorite. *Int J Rock Mech Min Sci Geomech Abstr* 9(4):513–516
- Quiñones J, Arzúa J, Alejano LR, García-Bastante F, Mas Ivars D, Walton G (2017) Analysis of size effects on the geomechanical parameters of intact granite samples under unconfined conditions. *Acta Geotech* 12:1229–1242
- Shi Q, Mishra B, Zhao Y (2022) DEM analysis of the effect of lamination properties on the stability of an underground coal mine entry with laminated shale roof. *Min Metall Explor* 39(2):495–506
- Simon R, Deng D (2009) Estimation of scale effects of intact rock using dilatometer tests results. In: 62nd Canadian Geotechnical Conference, Halifax. p 481–488
- Singh MM, Huck PJ (1972) Large scale triaxial tests on rock. In: The 14th US Symposium on Rock Mechanics (USRMS)
- Song H, Jiang Y, Elsworth D, Zhao Y, Wang J, Liu B (2018) Scale effects and strength anisotropy in coal. *Int J Coal Geol* 195:37–46
- Tani K (2001) Scale effect on shear strength of sedimentary soft rocks observed in triaxial compression test (influence of potential joints). In: 36th National Conference of the Japanese Geotechnical Society. p 597–598
- Weibull W (1939) A statistical theory of the strength of materials. Stockholm: Generalstabens litografiska anstalts förlag
- Yoshinaka R, Osada M, Park H, Sasaki T, Sasaki K (2008) Practical determination of mechanical design parameters of intact rock considering scale effect. *Eng Geol* 96:173–186
- Zhai H, Masoumi H, Zoorabadi M, Canbulat I (2020) Size-dependent behaviour of weak intact rocks. *Rock Mech Rock Eng* 53:3563–3587
- Zhao Y (2022) Size effect and anisotropy on the strength of shale under compressive stress conditions. Doctor's thesis. West Virginia University

Springer Nature or its licensor (e.g. a society or other partner) holds exclusive rights to this article under a publishing agreement with the author(s) or other rightsholder(s); author self-archiving of the accepted manuscript version of this article is solely governed by the terms of such publishing agreement and applicable law.